Simultaneous measurements of 3D temperature and velocity fields in gas flows using thermographic phosphor tracer particles

Moritz Stelter[1,*], Fabio J. W. A. Martins[1,2], Frank Beyrau[1] and Benoît Fond[1,3]

1: Institute of Fluid Dynamics and Thermodynamics, Otto von Guericke University Magdeburg, Germany
2: Current address: Institute for Combustion and Gas Dynamics, University of Duisburg-Essen, Germany
3: Current address: ONERA – The French Aerospace Laboratory, Meudon, France
*Corresponding author: moritz.stelter@ovgu.de

Keywords: 3D measurements, 3D-PTV, thermographic phosphors, flow thermometry, multivariable measurements, gas flow

ABSTRACT

A concept for joined three-dimensional temperature and velocity measurements in turbulent gas flows using sub-micron sized thermographic phosphor tracer particles is presented. Such measurements are needed to resolve flow structures commonly encountered in turbulent flows of scientific and industrial interest. While available techniques for simultaneous 3D thermometry and velocimetry are suitable for microfluidic applications or slow liquid flows, the present concept is applicable to macroscopic turbulent gas flows. The feasibility of these measurements is demonstrated using two turbulent heated gas jets. The concept utilizes two sub-systems: a four-view 3D particle tracking velocimetry system combined with a two-view ratiometric phosphor thermometry system. A double-pulse green laser and a single-pulse UV laser are used for illumination and excitation of phosphor luminescence, respectively. Upon imaging the particle-laden flow using the joined camera system, 3D particle positions and velocities are computed from four double-frame Mie-scattering recordings, while the temperature is inferred from two single-frame luminescence-emission recordings. Measurement results using low particle seeding density successfully retrieve the expected temperature and velocity distributions. This proof-of-concept is a first step towards the ability of resolving 3D turbulent flow structures from individual single-shot recordings using higher particle seeding densities.

1. Introduction

The study of turbulent flows is crucial to many industrial sectors reliant on convective heating or cooling, mixing or dispersion of substances, as well as to fundamental research in stratified flows occurring in the atmosphere or oceans. Such flows are inherently three-dimensional and characterized by spatial and temporal fluctuations in flow velocity over a wide range of scales. These properties prompted the development of three-dimensional velocity measurement techniques based on imaging tracer particles within the flow using multiple cameras and reconstructing the particle distribution in 3D. Then, either individual particles or intensity patterns created by particle

ensembles are tracked from frame to frame in particle tracking velocimetry (PTV) or in particle image velocimetry (PIV), respectively. Nowadays, three-dimensional three-component velocity measurements in gas and liquid flows are possible using these techniques at low (Hz) and high (kHz) sampling rates, at micrometer to meter scales (Discetti & Coletti, 2018; Scarano, 2012).

Yet velocity measurements alone are not always sufficient to describe the transport of heat and mass in turbulent flows (Warhaft, 2000) and simultaneous scalar measurements (e.g., temperature or species concentration) are needed to develop appropriate models. These measurements typically rely on scattering and luminescence processes of molecules, such as Rayleigh scattering or laser induced fluorescence. Their extension to three-dimensional measurements requires either a scanning approach (Krug et al., 2014), with limited temporal resolution due to the finite scan time, or a multi-view tomographic reconstruction of volumetric signals (Yu et al., 2017), which could lead to biased statistics due to low-pass filtering over unresolved turbulent fluctuations in each elemental reconstruction volume. Ultimately, for combined 3D scalar and velocity measurements using such approaches, at least two multi-view systems must be combined typically yielding different reconstructed geometries.

Another approach is to use seeded particles within the flow for both, 3D temperature and 3D velocity measurements, as proposed here and in two recent studies using different concepts. Massing et al. (2018) performed microscopic astigmatism PTV coupled with a double-frame lifetime determination of encapsulated EuTTA particles to study a liquid micro-channel flow. In another study by Schiepel et al. (2021), 100 µm thermochromic liquid crystal particles were dispersed in a Rayleigh-Bénard convection cell filled with a water-glycol mixture. Images of the particles illuminated by white light were captured by four monochrome cameras for tomographic particle image velocimetry and 3D particle localization, as well as by a color camera with stopped-down aperture to determine temperature from their Hue value. Both approaches result in scattered measurements of temperature and the three components of velocity at each 3D particle location with no temporal or spatial filtering.

While being well suited for micro fluidics and slow flows at ambient temperatures in liquids, the mentioned techniques are not applicable to macroscopic turbulent flows in gases due to their particles' long response times. Here, we propose to use sub-micron thermographic phosphor particles, which exhibit temperature-dependent luminescence properties with response times in the microsecond range and excellent thermochemical stability, making them ideal tracers for turbulent flows. These particles have been used for planar measurements in turbulent flows up to 900 K (Abram et al., 2018). Now, we aim to extend their applicability to 3D measurements. For this purpose, Mie-scattering images are captured by four cameras for 3D particle position reconstruction and velocimetry, while two additional cameras are used for two-color ratiometric temperature measurements. The temperature information is derived from macroscopic images of individual sub-micron particles, which is a major challenge compared to the above-mentioned studies where large particles or microscopic imaging could afford much higher signal levels. In the following, the imaging method, the employed tracer particles and the developed setup are described. The

results of demonstration experiments to provide simultaneous 3D temperature and velocity measurements in turbulent heated gas jets are also presented.

2. Experimental setup

ZnO particles (Sigma Aldrich 96479) with a volume equivalent diameter of 600 nm are chosen as flow tracers for this study. Their response time is estimated to below 5 µs (Straußwald et al., 2020). Upon excitation using ultraviolet light, they emit a luminescence signal with a lifetime below 10 ns, centred at 387 nm at 293 K. The emission spectrum exhibits a red-shift with increasing temperature as shown in Fig. 1b. This shift is exploited for temperature measurements using the intensity ratio approach (Abram et al., 2018). Two cameras image the particles through spectral filters with transmission profiles as shown in Fig. 1b so that the ratio between both cameras' image intensities is a sensitive and monotonic function of temperature. Due to the short luminescence lifetime and the fast particle response time, these ZnO particles can be applied in a wide range of turbulent flows without turbulence demodulation or motion blurring (Straußwald et al., 2020).

The optical setup used in the present work is depicted in Fig. 1a. To facilitate simultaneous three-dimensional particle-based temperature and velocity measurements in gas flows, particle positions need to be reconstructed first and then the luminescence emission from these particles is evaluated for temperature measurements. Finally, reconstructing particle positions from images recorded shortly after one another allows the computation of three-dimensional particle displacements and therewith particle velocities. A double-pulse 10 Hz Nd:YAG laser is operated at 532 nm to illuminate the particles for position reconstruction and PTV measurements. Particle Mie-scattering images are captured by four cameras (LaVision Imager pro X) P1 to P4 to allow 3D particle position reconstruction and velocity measurements using in-house algorithms. These cameras are positioned on a common horizontal plane at angles of 51°, 67°, 113° and 129°, where 0° is the forward scattering direction. They are equipped with Scheimpflug adapters and 100 mm focal length objectives. Their apertures are set to $f/22$ for P1 and P2 and to $f/16$ for P3 and P4, respectively, to produce sharply focused particle images over the whole measurement volume.

To excite the luminescence from ZnO particles for thermometry measurements, a single-pulse 10 Hz Nd:YAG laser is employed at 266 nm. This laser is operated at high fluence, exceeding 200 mJ/cm^2 in a 8 mm diameter beam, to saturate the phosphor and make its emission spectrum insensitive to fluence fluctuations (Abram et al., 2015). A telescope (T) was used to match the diameter of the green beams and the ultraviolet laser beam. All laser beams are overlapped using a dichroic mirror and then the low-fluence beam edge is removed using a circular aperture. To facilitate temperature measurements from the phosphor luminescence emission, two cameras (LaVision Imager sCMOS) T1 and T2 are equipped with distinct spectral filters (cf. Fig. 1b). These cameras are positioned on the same horizontal plane as the PTV cameras at angles of 90° and 100°. Both cameras are equipped with Scheimpflug adapters and 85 mm objectives to match the magnification of the PTV cameras at 0.2. To maximise luminescence signal collection the apertures are

opened up to $f/1.4$. As a result, not all particles within the illuminated volume are imaged in focus with implications for the image processing as discussed below.

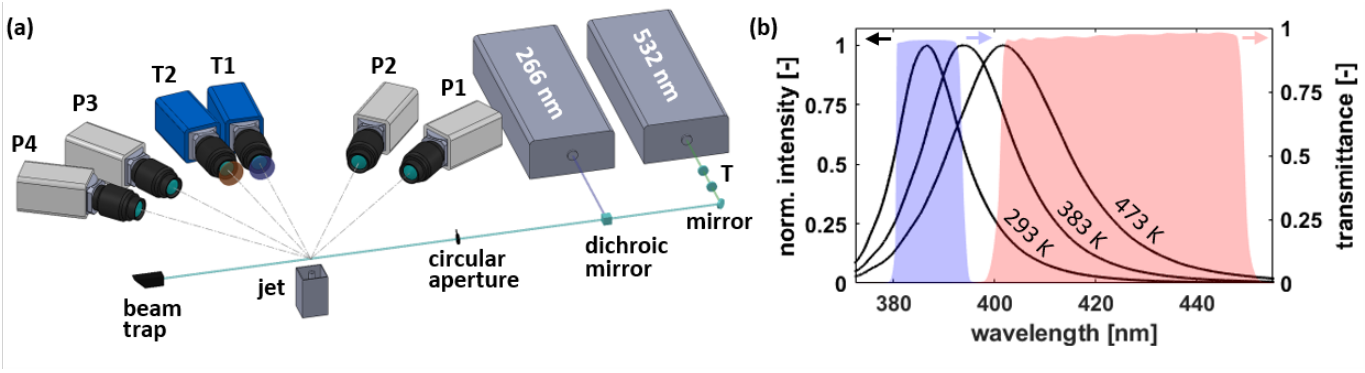

Figure 1. (a) Schematic of the experimental setup consisting of six cameras, two lasers, optical components and the jet nozzle with co-flow section. (b) Luminescence emission spectra of ZnO at three different temperatures together with normalized transmission profiles of the filters used for cameras T1 and T2.

To perform simultaneous temperature and velocity measurements, the first green and the ultraviolet laser pulses are fired synchronously, while the delay between both green laser pulses is adjusted depending on the flow conditions. Cameras P1 to P4 are operated in double-frame mode whereas cameras T1 and T2 are operated in rolling shutter mode, to minimise camera readout noise and to improve the signal to noise ratio of weak luminescence images. An exposure time of 35 ms for T1 and T2, starting 32 ms before the first laser beams, yields a common exposure time of all sensor rows of about 5 ms within which the ultraviolet laser is fired, creating a global-shutter-like image in rolling shutter operation. The measurements are taken at 5 Hz limited by cameras P1-P4 (i.e., capturing images every second laser pulse). Summarizing, six simultaneous images (four Mie-scattering and two luminescence images) of the particles are recorded at the first pulse time and four Mie-scattering images are captured during the second pulse time.

3. Processing

3.1. Camera calibration

To allow successful determination of three-dimensional particle positions from multiple 2D projections, an accurate camera calibration is required. A pinhole-based camera model is used to map 3D world coordinates of the reconstruction volume into 2D image coordinates. A custom made planar dot-target with a 5x5 mm^2 grid is precisely translated over nine positions along the in-depth axis (z-axis, aligned with the optical axis of camera T1) using a micrometer stage. To increase the depth of field of cameras T1 and T2 while preserving the validity of the calibration, external apertures are placed in front of their entrance pupils which are closed during target image acquisition without touching the cameras or lenses themselves.

3.2. Tomographic reconstruction

Particle positions are retrieved from reconstructed volumes based on Mie-scattering intensity distributions as captured by cameras P1-P4. To allow three-dimensional particle position reconstruction, the measurement volume is discretized into approx. $900 \times 180 \times 340$ voxels composed of cubic voxels of 40 µm. A fast non-iterative minimum line of sight (MinLOS) method (Putze & Maas, 2008) is employed in the present assessment of the technique with a low seeding density (<0.01 particles per pixel). More sophisticated reconstruction methods will be employed in the future with intermediate to high seeding densities. The camera images are pre-processed as follows: (i) background subtraction, (ii) Gaussian smoothing, (iii) local peak detection above a noise-floor threshold, (iv) sub-pixel peak position refinement based on 2D Gaussian fit and (v) generation of synthetic images of Gaussian particle blobs at the detected sub-pixel peak locations. This reduces the influence of the laser beam profile on the Mie-scattering images. As the particle images in cameras P1-P4 are diffraction-limited, a Gaussian fit is well suited to model their particle image intensity distributions (Airy disk). To remove spurious particle images, a filter based on the standard deviation of the Gaussian fit is applied. From the pre-processed images, the volume reconstruction is performed using the MinLOS implementation. The reconstructed volumes are smoothed and low intensity regions zeroed, before determining 3D particle positions by the center of gravity of connected 3D regions for sub-voxel precision. These 3D positions are then projected into each camera image, as illustrated by distinct red markers in Fig 2a and b. These projections are then paired to particles identified in the individual camera images, both from luminescence as well as from PTV cameras (green circles in Fig. 2a and b), and only particles paired in all cameras are kept for further processing.

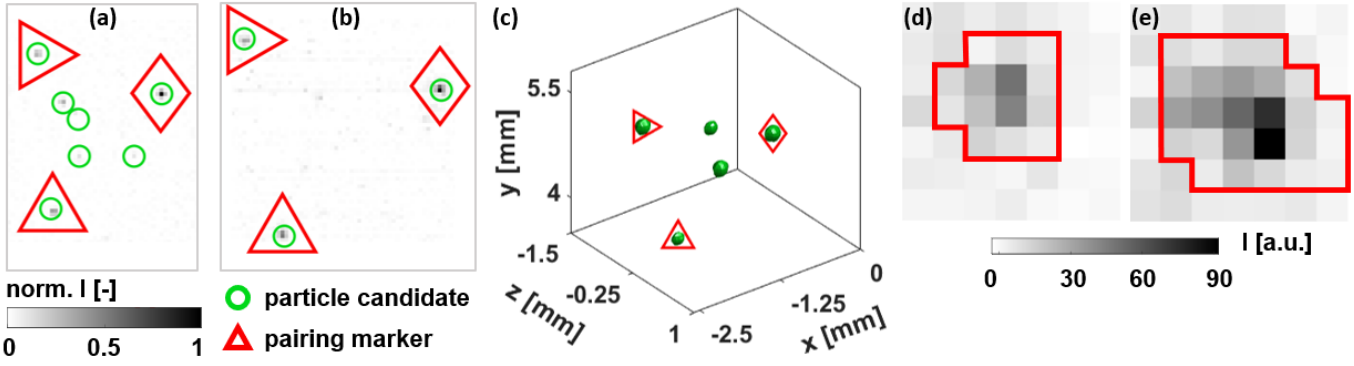

Figure 2. Examples of zoomed-in simultaneously-acquired Mie-scattering (a) and luminescence images (b) are shown in normalised intensity grey scale from cameras P3 and T1 respectively, together with green isosurfaces of particle intensities in the corresponding reconstructed volume (c). A selected luminescence particle image pair with the signal integration region marked by a red contour is presented in (d-e).

As the luminescence cross-section is orders of magnitude lower than the Mie-scattering cross-section, signal levels in the luminescence images are much lower. As a result, about 3.5 times fewer particles are successfully paired in the luminescence images compared to Mie-scattering images. Depth-dependent blur and aberrations in the luminescence images contribute to a broader

distribution in particle image peak intensities compared to diffraction-limited scattering images. Therefore, many particles with low peak intensities are not detected in luminescence images.

3.3. Temperature evaluation

To derive particle temperatures in the present approach, the luminescence emission of each particle must be evaluated from the images of both luminescence cameras. This is necessary to compute per-particle intensity ratios, which can be converted to temperature. Therefore, each reconstructed particle position is projected into the images of both cameras T1 and T2. Around these positions a region of 2 pixel is interrogated to find the closest local particle image. To determine the pixels containing the luminescence signal an adaptive mask is used, as shown in Fig. 2d and e. The mask is obtained by evaluating a two-dimensional Gaussian fit of the local particle images and summing all pixel intensities where the fitted value is above 5 % of the fit maximum. To account for random particle image orientation with respect to the image axes, a generalized rotation-enabled Gaussian fit is used, allowing elliptical masks. Intensity ratios are calculated for each individual particle by dividing the sum of pixel intensities from T2 by those from T1.

To convert these intensity ratios to temperature values, an in-situ calibration is performed using a 9.5 mm diameter heated jet. 3D intensity ratio fields are measured at four different jet exit temperatures from 295 K to 438 K. Results accumulated over several images for each calibration temperature are plotted in Fig. 3a-d. As expected, the ratios of particles in the jet core increase with increasing temperature, whereas lower ratios are found at larger radial distance to the jet center. For calibration, the intensity ratios of particles found in a 2.5 mm-diameter sub-volume in the jet center are ensemble averaged to provide the calibration points shown in Fig. 3e. A power-law curve fit of the form of $\varphi(T) = p_1 + p_2 \cdot T^{p_3}$, with φ being the intensity ratio and T the temperature, is applied to provide the ratio-to-temperature conversion relation.

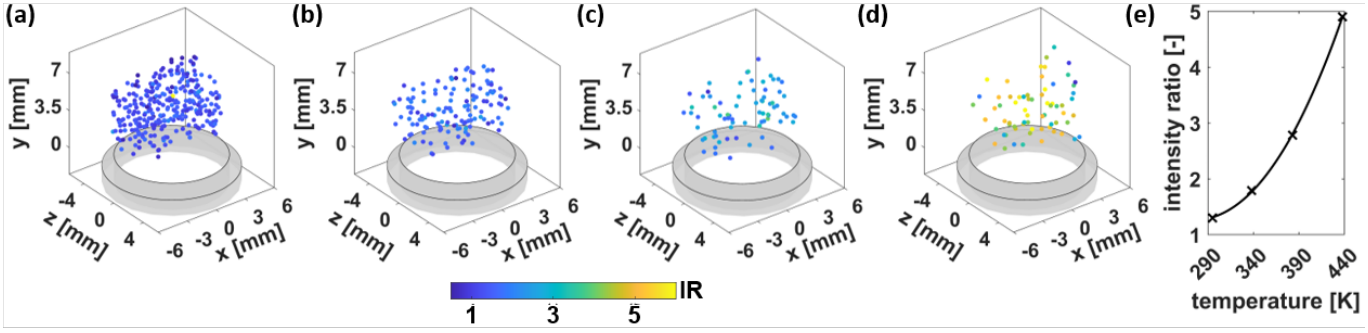

Figure 3. Accumulated intensity ratio distributions at jet exit temperatures of 295 K (a), 338 K (b), 383 K (c) and 438 K (b), and ratio-to-temperature conversion curve (e).

3.4. Velocity evaluation

The processing steps to obtain three-dimensional velocity data are outlined in the following. As a first step, volume reconstruction of three-dimensional particle positions is performed using the Mie-scattering images recorded by cameras P1-P4 during both green laser pulses. A first guess of each particle's displacement is obtained from multi-pass cross-correlation of the ensemble reconstructed volume pairs (Kováts et al., 2020). Then, each individual particle displacement is determined from instantaneous volume pairs by simply searching for the closest corresponding particle in the second time-step volume within a maximum distance of 2 voxel around the guessed position. This is possible due to the low seeding density used here. A more sophisticated 3D PTV method can be used in the future with intermediate to high seeding densities for solving the then non-negligible number of ambiguous particle pairings. Finally, converting the particle displacement in voxels to world units and dividing it by the known time delay between both green laser pulses yields the desired velocity information.

4. Results

Demonstration measurements are performed in two heated gas jets of 4 mm and 9.5 mm in inner diameter surrounded by a co-flow, referred to as small and large jets. The jets are heated to a nozzle exit temperature of 383 K at bulk velocities of 28 m/s and 11.75 m/s respectively, resulting in a Reynolds number of 4600, while the co-flow remains at room temperature and low velocity of 0.2 m/s. All streams are seeded with sub-micron ZnO particles. A typical single-shot combined measurement of temperature and velocity in the small jet is shown in Fig. 4 for a zoomed-in region. Particles within the jet indicate a temperature close to the nozzle exit temperature and high velocities around the jet bulk velocity. Particles in the co-flow appear with low temperature and velocity. As a very low seeding density was used for this demonstration only few particles are captured per single-shot recording.

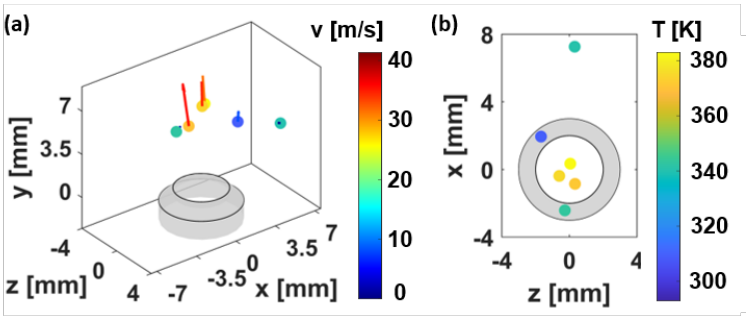

Figure 4. Typical instantaneous temperature and velocity results from the small heated jet surrounded by a room-temperature co-flow in 3D (a) and top view (b).

To obtain dense, time-averaged temperature and velocity distributions, measurements from more than 1000 single-shots were combined. Such accumulated fields for the large jet are presented in

Fig. 5. Velocity and temperature results are shown in 3D (a,d) and top view (b,e), as well as in a height versus radial distance scatter plot (c,f). Due to the much lower signal strength of luminescence compared to Mie scattering and an associated difference in detectability of particles in scattering and luminescence camera images, eight times more particles could be used for velocity measurements than for temperature measurements. This is reflected by the number difference in velocity and temperature samples in fig. 5. The velocity data shows excellent symmetry about the jet axis with a relatively uniform velocity magnitude in a 2 mm diameter core region. A flow velocity of approx. 14 m/s is found within this region, corresponding to 119 % of the bulk velocity, as expected from the one-seventh power-law for turbulent pipe flows (Chant, 2005), before it drops steeply towards the ambient co-flow velocity within a thin shear layer. The temperature data shows a similar axis symmetry, but the data is noisier. No post-processing filters are applied. Particles indicating a high temperature are grouped within the central region of the jet while particles in the co-flow indicate low temperatures with a sharp transition between both regions. Particles in the co-flow at positive x- and z-positions express higher than ambient temperatures. This seems to be due to back-reflections from the nozzle wall and emissions of hot particles stuck to the inner wall of the nozzle, as the laser beams are propagating along the x-axis towards negative direction. Increasing the distance between nozzle and laser beams removes this artifact. The particle-to-particle temperature precision within one standard deviation evaluated in the jet core region is 18 K.

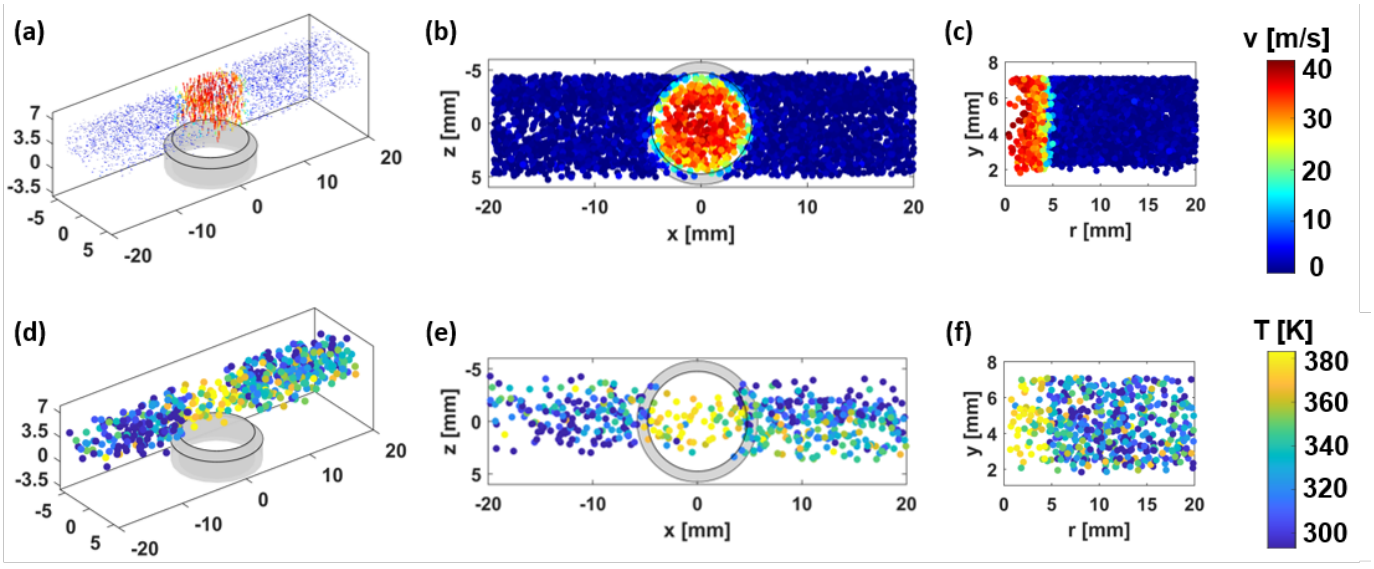

Figure 5. Temperature and velocity results from accumulated instantaneous measurements in the large heated jet surrounded by a room-temperature co-flow are presented in 3D (a,d) and top view (b,e). (c,f) The rotational symmetry of temperature and velocity distributions about the jet axis is shown in height versus radial distance scatter plots of temperature and velocity data.

While these results demonstrate the applicability of the developed technique to turbulent gas flows, higher particle seeding densities are desired for increased spatial resolution. More advanced reconstruction algorithms can handle particle images with seeding densities exceeding 0.1 particles per pixel (ppp) as reported by Michaelis et al. (2010), compared to approx. 0.0016 ppp for the

presented measurements. However, the particle image size in the luminescence images is larger than that in the PTV images, which may impose an upper limit on the particle seeding density if only non-overlapping particle images are considered as usable. To provide an estimate of the maximum seeding density, virtual particle images are used from which the amount of unambiguously identifiable and non-overlapping luminescence particles can be evaluated. Artificial particles are randomly distributed within a volume of $70 \times 70 \times 7$ mm^3 at multiple seeding densities. The relation between particle image diameter in the luminescence images and its z-position in the 3D volume is derived from results of the Gaussian fits (particle diameter = $4\,\sigma$) of particle images obtained in an isothermal jet at two different apertures. The resulting function is shown for $f/1.4$ in Fig. 6a. Artificial luminescence images are then generated from these distributions as particle image blobs using 2D Gaussian fits with diameters according to the particle z-position dependency. The number of usable particles and the separation ratio (i.e., ratio between unambiguously identifiable and non-overlapping particle images with respect to the total number of particles) is calculated for two luminescence camera lens apertures of f/1.4 and f/2.0. Results are presented in Fig. 6b. It is observed that there is an optimum at a seeding density of 0.022 ppp for the currently used aperture of f/1.4. Increasing the particle seeding density beyond this level leads to a lower number of usable particles due to increasing overlap of individual particle images. Implementing volume self-calibration (Wieneke, 2008) and advanced volume reconstruction algorithms (Cornic et al., 2020; Wieneke, 2012) should allow us to process images at this seeding density, offering an approx. 20-fold improvement in spatial measurement density compared to now.

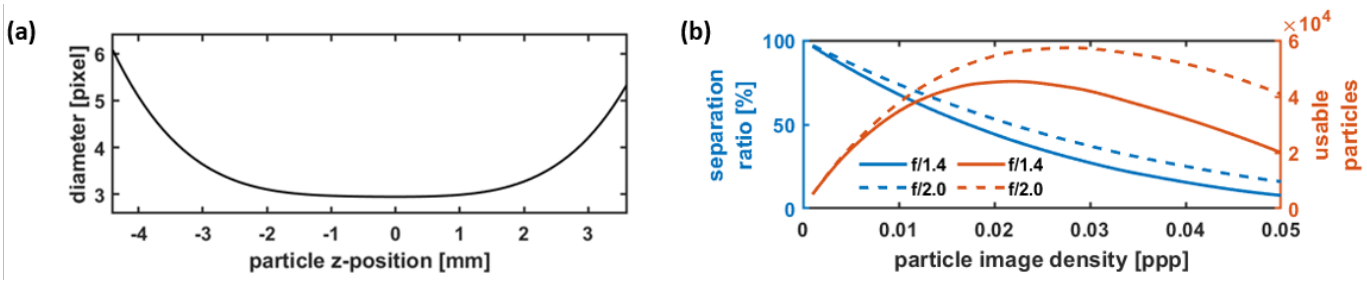

Figure 6. (a) Particle image size versus particle z-position as determined from particle image recordings at f/1.4 aperture. Particle image diameter is estimated as 4 σ of a 2D Gaussian fit. (b) Separation ratio and absolute number of usable particle images for different seeding densities and two luminescence camera apertures from a simulated domain of $70 \times 70 \times 7$ mm^3.

5. Conclusions

A new technique for simultaneous three-dimensional temperature and velocity measurements based on sub-micron thermographic phosphor tracer particles is developed and demonstrated in turbulent heated gas jets. The setup is composed of six cameras and two lasers. The technique allows the temperature and the three components of velocity of turbulent flows to be determined at every reconstructed particle position within the volume (for paired particle images in all cameras) avoiding spatial bias effects and filtering. Demonstration measurements at low seeding density

(0.0016 ppp) provided a few measurements per shot of joint temperature and three component velocity. Accumulated measurements successfully retrieved the symmetry about the jet axis of temperature and velocity distributions.

Further research focuses on increasing the particle seeding density towards the estimated limit of 0.022 ppp to provide measurements with higher spatial density. This will be achieved by implementing more advanced volume reconstruction methods. Additionally, particles with a narrower size distribution, higher luminescence signal emissions and potentially less variability in luminescence emission properties are currently being investigated to equalize the number of temperature and velocity samples. This will help to improve the results towards instantaneous measurements of coherent three-dimensional flow structures within dynamic flow fields.

Acknowledgements

Funding by the Deutsche Forschungsgemeinschaft (DFG, German Research Foundation) under project number 427979038 is gratefully acknowledged.

References

Abram, C., Fond, B., & Beyrau, F. (2015). High-precision flow temperature imaging using ZnO thermographic phosphor tracer particles. *Optics Express*, *23*(15), 19453.

Abram, C., Fond, B., & Beyrau, F. (2018). Temperature measurement techniques for gas and liquid flows using thermographic phosphor tracer particles. *Progress in Energy and Combustion Science*, *64*, 93–156.

Chant, L. J. D. (2005). The venerable 1/7th power law turbulent velocity profile: a classical nonlinear boundary value problem solution and its relationship to stochastic processes. *Applied Mathematics and Computation*, *161*(2), 463–474.

Cornic, P., Leclaire, B., Champagnat, F., Besnerais, G. L., Cheminet, A., Illoul, C., & Losfeld, G. (2020). Double-frame tomographic PTV at high seeding densities. *Experiments in Fluids*, *61*(2).

Discetti, S., & Coletti, F. (2018). Volumetric velocimetry for fluid flows. *Measurement Science and Technology*, *29*(4), 042001.

Kováts, P., Martins, F. J. W. A., Mansour, M., Thévenin, D., & Zähringer, K. (2020). Tomographic PIV measurements and RANS simulations of secondary flows inside a horizontally positioned helically coiled tube. *Experiments in Fluids*, *61*(5).

Krug, D., Holzner, M., Lüthi, B., Wolf, M., Tsinober, A., & Kinzelbach, W. (2014). A combined scanning PTV/LIF technique to simultaneously measure the full velocity gradient tensor and the 3D density field. *Measurement Science and Technology*, *25*(6), 065301.

Massing, J., Kähler, C. J., & Cierpka, C. (2018). A volumetric temperature and velocity measurement technique for microfluidics based on luminescence lifetime imaging. *Experiments in Fluids*, *59*(11).

Michaelis, D., Novara, M., Scarano, F., & Wieneke, B. (2010, July). Comparison of volume reconstruction techniques at different particle densities. In *15^{th} International Symposium on Applications of Laser Techniques to Fluid Mechanics.* Lisbon.

Putze, T., & Maas, H.-G. (2008). 3D determination of very dense particle velocity fields by tomographic reconstruction from four camera views and voxel space tracking. In *The International Archives of the Photogrammetry, Remote Sensing and Spatial Information Sciences.*

Scarano, F. (2012). Tomographic PIV: principles and practice. *Measurement Science and Technology*, *24*(1), 012001.

Schiepel, D., Schmeling, D., & Wagner, C. (2021). Simultaneous tomographic particle image velocimetry and thermometry of turbulent Rayleigh–Bénard convection. *Measurement Science and Technology*, *32*(9), 095201.

Straußwald, M., Abram, C., Sander, T., Beyrau, F., & Pfitzner, M. (2020). Time-resolved temperature and velocity field measurements in gas turbine film cooling flows with mainstream turbulence. *Experiments in Fluids*, *62*(1).

Warhaft, Z. (2000). Passive scalars in turbulent flows. *Annual Review of Fluid Mechanics*, *32*(1), 203-240.

Wieneke, B. (2008). Volume self-calibration for 3D particle image velocimetry. *Experiments in Fluids*, *45*(4), 549–556.

Wieneke, B. (2012). Iterative reconstruction of volumetric particle distribution. *Measurement Science and Technology*, *24*(2), 024008.

Yu, T., Liu, H., & Cai, W. (2017). On the quantification of spatial resolution for three-dimensional computed tomography of chemiluminescence. *Optics Express*, *25*(20), 24093.